

**ORAL SESSION:
MICROSYSTEMS 2**

A MILLIMETRE SIZE WIRELESS TEMPERATURE SENSOR WITH DIGITAL CONVERSION AND EMBEDDED 2.5GHz TRANSMITTER AND ANTENNA

Fabio Zito, Letizia Fragomeni, Francesco G. Della Corte
Dipartimento di Informatica, Matematica, Eletttronica e Trasporti (DIMET), Università degli Studi "Mediterranea" di Reggio Calabria, Via Graziella Loc. Feo di Vito, 89060 Reggio Calabria - Italy
 [fabio.zito] [letizia.fragomeni] [francesco.dellacorte]@unirc.it

Abstract

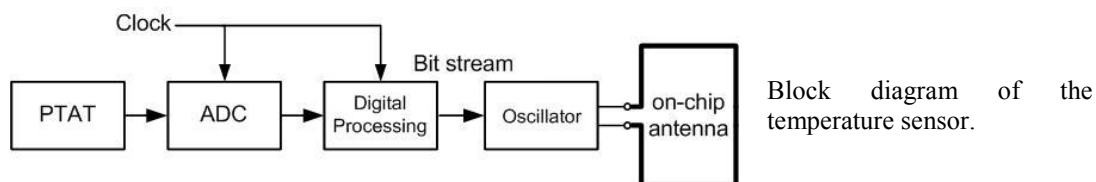
The feasibility of fully integrated wireless systems has already been demonstrated in several applications [1] [2] [3]. The benefits of having the integration of the radiating element are known and include substantially the small chip dimension, the elimination of external connection and avoid additional process steps.

Due to the typical small chip dimension, only high frequency bands can use these antennas in optimum, i.e. resonating, conditions.

Although the chip dimension do not allow resonant radiating elements, nevertheless this does not seem to be a limit for the specific application in contactless sensing, where a short distance wireless link is sufficient [3].

In this paper an improvement of a wireless temperature sensor with on-chip antenna [3] is presented. This solution, realized in 0.35 μ m CMOS technology, exploits a proportional to absolute temperature (PTAT) voltage scheme, where the difference between two base-emitter voltages under different bias current densities is constantly measured. The availability of bipolar transistors in CMOS technology allows to exploit their properties in temperature sensor applications.

The sensitivity, signal level and linearity of the sensor interface were specially conditioned in order to simplify further an Analog-to-Digital conversion (ADC). The idea is to convert the analog signal, i.e. the PTAT voltage, to a 8-bit digital signal, where each bit can modulate a Radio Frequency (RF) carrier generated by a Cross-Coupled oscillator, using an On-Off Keying (OOK) modulation.

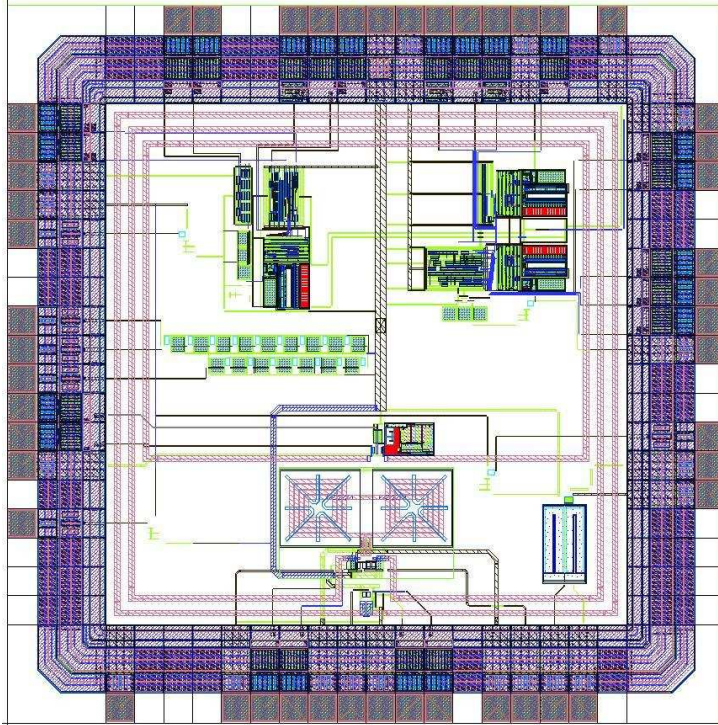


The signal is transmitted by a small loop antenna realized with the top metal level (i.e. aluminium) on the surface of the chip.

The electronic design of the sensor has been carefully tuned to get a linear voltage vs. temperature dependence for a wide temperature range (room temperature to 100°C), with a linear sensitivity of +10.62mV/°C. The analog input voltage is then converted using a 8-bit ADC (256 levels). For temperature the interval between 20°C to 100°C, we have a range of about 80°C. The analog signal has a swing of 810mV, with a resolution of about 3mV, which translates into an error of 0.3°C.

The bias voltage for the device is 3.3 V with a low DC current consumption of about 70 μ A for the PTAT sensor in continue operation mode.

About the analog-to-digital conversion and digital processing, the dynamic power consumption does not represent a considerable value in terms of dissipated power because the temperature is periodically acquired with a very long time interval, for example at 1Hz or less.



Test chip layout. The area is $2480\mu\text{m} \times 2480\mu\text{m}$.

About the RF-section, the carrier of the implemented oscillator is at 2.53GHz. The frequency stability with temperature and bias voltage allows its use in conjunction with a commercial receiver. This new solution has been designed in order to solve some problem shown in [3] concerning the frequency dispersion among different chips, which can be a reflex of process tolerances. These variations generally affect key parameters such as the threshold voltage, the transistor aspect ratio, the resistance values, and so on.

REFERENCES

1. Kenneth K. O et al., "On-Chip Antennas in Silicon ICs and Their Application", *IEEE Trans. On Electron Devices*, vol. 52, no. 7, pp 1312-1323, Jul. 2005.
2. K.K. O et al., "The Feasibility of On-Chip Interconnection using Antennas", *Computer-Aided Design*, 2005 IEEE.
3. F.Aquilino, M.Merenda, F.Zito, F.G.Della Corte, *2.4GHz Fully Integrated Wireless Temperature Sensor with On-Chip Antenna*, Proc. of the XIII AISEM Conference on Sensors and Microsystems, 2008

FABRICATION OF PLANAR SUB-MICRON SCHOTTKY DIODES FOR TERAHERTZ IMAGING APPLICATIONS

Francesco Gatta, Arnaldo D'Amico, C. Di Natale
*Dipartimento di Ingegneria Elettronica, Università degli studi di Roma "Tor Vergata",
via del Politecnico 1, 00133 Roma*

Michele, Ortolani, Ennio Giovine, Donatella Dominijanni, Vittorio Foglietti
*Istituto di Fotonica e Nanotecnologie, Consiglio Nazionale delle Ricerche,
via Cineto Romano 42 00156 Roma*

Abstract

Imaging sensors employing radiation at frequencies beyond the visible range are crucial in safety and security applications, as threats may come from concealed objects or internal material defects which cannot be detected by visual inspection. Infrared radiation can be conveniently used for night vision and thermal imaging, but sub-millimeter waves and terahertz radiation (frequencies from 100 to 3000 GHz) is necessary for more demanding applications requiring stand-off, non-destructive sensing, due to its much larger penetration depth into packages, clothes and dielectric materials. Possible application areas for terahertz sensing are very diverse: safety tests of structural components of aircrafts, mail inspection, passenger screening at security gates [1].

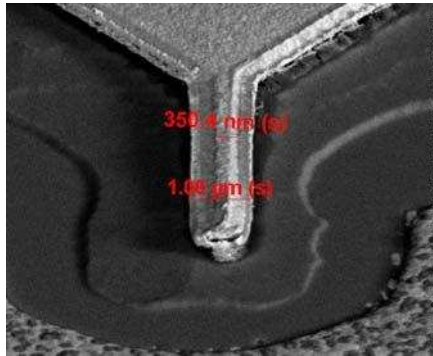
At present, competing technologies with large penetration capabilities involve the use of X-rays or high magnetic fields, which involve risks for the health of target people and operators. On the other side of the electromagnetic spectrum, microwave and radiofrequency (RF) devices using radiation up to several tens of GHz are currently employed for security sensing (e.g. in RF metal detectors), but they can hardly detect the shape of the concealed object, as the resolution of microwave imaging is limited by diffraction.

In this context, there is a considerable effort to bring concepts and devices from both the microwave and the infrared range towards the terahertz range, which sits in between them, with the aim of performing standoff imaging of concealed objects. In this paper, we present a process for the fabrication of Schottky diodes which can operate in the terahertz range. The Schottky diode is based on a metal-semiconductor junction and has rectifying properties. If an electromagnetic signal is fed to the diode through an antenna, there will be a dc output proportional to the intensity of the electromagnetic field (operation as a video detector). Indeed, Schottky diodes are currently employed as sensors of microwave radiation up to 100 GHz, but their fabrication process has to be strongly modified to make them sensitive to terahertz radiation [2], as we will show in this paper. Furthermore, our process is also compatible with the fabrication of matrixes of radiation detectors which could then be used to acquire real-time terahertz images in a focal plane array configuration, similar to infrared vision devices or digital cameras.

The main parameter which limits the operation frequency of the Schottky diode is the junction capacitance, which is proportional to the junction area. Sub-micron junctions are needed for terahertz operation, which can be fabricated by high-resolution electron-beam lithography, instead of conventional optical lithography. Parasitic capacitances between the contact pads are also a problem, which can be solved by using air-bridge fabrication technology, physically decoupling the contact pads, leaving a micrometric metal bridge for connection between them. A third parameter limiting the cut-off frequency is the series resistance, which can be reduced by using high-electron mobility Gallium Arsenide (GaAs) epitaxial layers as the semiconductor material, instead of silicon. The resulting device is a fully planar monolithic Schottky diode working at terahertz frequencies which can be fabricated in arrays on a semiconductor wafer for imaging applications.

The Schottky diode is fabricated on a GaAs wafer with a layer structure on top, purposely grown by molecular beam epitaxy. On the GaAs semi-insulating substrate, a 1-micron thick n^+ -doped ($N_D=5e18$) and a 0.1 micron thick n -doped ($N_D=1e18$) GaAs layers have been grown. An evaporated metal layer on the n -doped GaAs forms the anode (metal side of the junction). A different metallization process on the n^+ -doped layer is used for the ohmic contact to the cathode (semiconductor side of the junction). The device is then isolated by mesa etching in order to interrupt the electric connection through the n^+ -layer which exists between different devices and between the anode and the cathode. Moreover, the large capacitor associated

with the anode contact pad can be decoupled by fabricating the diode on two separate mesas. The anode contact pad is located on one mesa, whose only purpose is the mechanical support of the pad, while the other mesa hosts both the Schottky junction and the ohmic contact pad to the cathode. A single gold-titanium bilayer is used for the anode, formed by a large contact pad on the first mesa, a micrometric air-bridge between the mesas and a sub-micron finger on the second mesa. The Schottky junction area must be as small as possible, however not affecting too much the contribution to the series resistance and inductance due to the anode metal finger. For these reasons the Schottky junction has been realized by employing “T-Gate” technology, developed for high-frequency transistors based on compound semiconductors. This “T” shaped section of the metal anode allows contacting small areas, thus obtaining a small junction capacitance, keeping at the same time the series resistance low, through the widening of the metal cross section [3].



Scanning Electron Micrograph of the Ti/Au “T-Gate” finger, which forms the Schottky junction to the n -doped GaAs layer. The junction is surrounded by the ohmic contact pad, characterized by a rough surface.

The manufacturing process of the device begins with the formation of the ohmic contact. The n^+ -layer to be contacted is reached through a wet recess etch of the n -layer. The etching mask has been realized with a photoresist on which the ohmic contact area has been opened by optical lithography. Immediately after the recess, the germanium-gold multilayer needed for ohmic contact formation on GaAs has been deposited by electron-gun evaporation followed by a nickel layer and a final thick gold layer deposition. The nickel layer has the unique scope to avoid diffusion of the underlying metals in the gold layer above. An acetone lift-off step is used to dissolve the photoresist, thus removing the metals outside the contact area. The actual ohmic contact formation is made through a 400°C bake which melts the multilayer to form an alloy, and allows its diffusion in the underlying n^+ -doped semiconductor, increasing the doping level.

The anode contact realization has been entirely made with the aid of electron-beam lithography instrumentation (Leica Electron Beam Pattern Generator 5 HR). A tri-layer of resist polymers with different sensitivities to electronic dose has been spin-coated on the wafer. By regulating EBL doses it is possible to selectively impress the different polymer layers, thus obtaining “T” profile for the anode contact. Once the pattern is generated, a first titanium deposition followed by a thick gold deposition are performed. A subsequent acetone lift-off removes the resist polymers and the metals above, leaving the anode contact on the wafer.

Finally the junction area is protected by photoresist with a further optical lithography step, and wet etching of the GaAs substrate is performed. This forms the two isolation mesas, leaving the metal air bridge suspended between them. The contact pads have been shaped to form planar antenna structures and diodes are fabricated at a distance of 3 mm to each other, to produce a monolithic detector array for 220 GHz. Test measurements are ongoing.

In conclusion, we reported on the fabrication of Schottky diodes working at terahertz frequencies, to be used in a detector array configuration for terahertz imaging applications. The process has been set up to be fully lithographic and planar, to allow future industrial exploitation.

REFERENCES

1. Peter H. Siegel, Terahertz Technology, IEEE Transactions on Microwave Theory and Techniques, vol. 50, no. 3 (March 2002).
2. Thomas W. Crowe, Robert J. Mattauch, Hans Peter Roeser, William L. Bishop, William C. B. Peatman and Xiaolei Liu, GaAs Schottky Diodes for THz Mixing Applications, Proc. Of IEEE vol. 80, no. 11 (November 1992).
3. Peter H. Siegel, R. Peter Smith, Michael C. Gaidis, Suzanne C. Martin, 2.5-THz GaAs Monolithic Membrane-Diode Mixer, IEEE Transactions on Microwave Theory and Techniques, vol. 47, no. 5, pp. 596-604 (May 1999)

FIBER OPTIC BROADBAND ULTRASONIC PROBE FOR VIRTUAL BIOPSY: TECHNOLOGICAL SOLUTIONS

Stefano Cerbai, Elena Biagi, Leonardo Masotti

*Dipartimento di Elettronica e Telecomunicazioni (DET), Università degli Studi di Firenze, via S. Marta, 3,
50139 Firenze, Italy*

Luca Belsito, Alberto Roncaglia

Istituto per la Microelettronica e Microsistemi (IMM-CNR), via Gobetti, 101, 40129 Bologna, Italy

Niccolò Speciale, Guido Masetti

*Dipartimento di Elettronica, Informatica e Sistemistica (DEIS), Università di Bologna, viale Risorgimento, 2,
40136 Bologna, Italy*

Abstract

Background, motivation, objective

Our group proposed the design and realization of an ultrasonic source based on opto-acoustic effect in 1996, with a metal layer over the fiber optic tip as absorbing target. In 2001 we improved the opto-acoustic conversion by replacing the metal absorbing target with a graphite one. Two years later, in 2003, we proposed a complete opto-acoustic and acousto-optic setup for a fully fiber optic ultrasonic probe.

The proposed probe consists of two optical fibers: one generating ultrasounds by opto-acoustic conversion, the second one, based on acousto-optic effect, used to detect ultrasounds.

The intrinsic high frequency and wide band associated both to the opto-acoustic source and to the interferometric acousto-optic element could open a way towards a “virtual biopsy”.

“Virtual biopsy” is perspective to provide the physicians the possibility of studying the nature and health condition of small portions of living tissue “in situ” by using ultrasounds.

Contribution/Method

A Micro-Opto-Mechanical-System (MOMS) approach is proposed to realize miniaturized opto-acoustic probes on optical fibres, in which the optical emitters and receivers are realized on micromachined frames that can be subsequently mounted on the fibre tip in a self-aligned way.

For the ultrasound emitter, a carbonization procedure has been adopted on photoresist patterns to obtain amorphous carbon layers suitable for optoacoustic emission. For the receiver, Fabry-Perot interferometers composed by two thin metal layers (evaporated Al) and a SU-8 spacer have been realized using different thicknesses of the individual layers. The carbon, SU-8 and Al layers have been characterized with Raman, Fourier Transform Infrared (FTIR) and optical spectroscopy to determine their optical properties and in particular the spectral reflectivity of the SU-8 interferometers. Ultrasound emission of the carbon layers has been and the Fabry-Perot response has been evaluated.

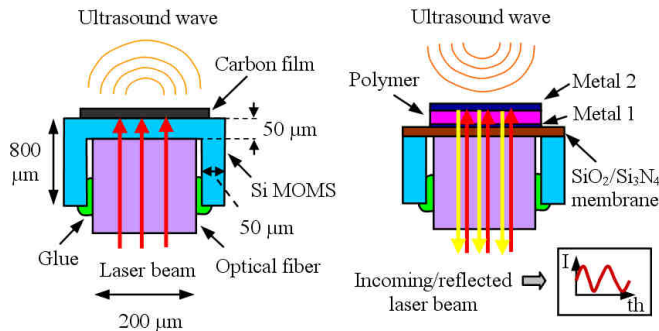
Results

We present our technological achievements in the development of the first all fiber optic probe and novel images of simple test objects, obtained with a complete opto-acoustic setup.

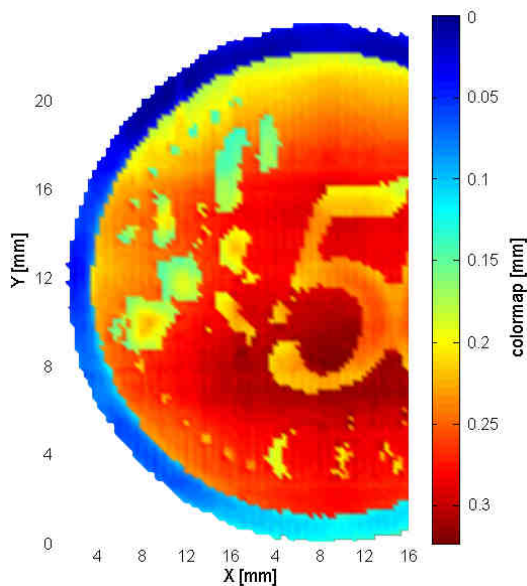
Discussion and conclusions

Prototypes realized with different solutions, both for the transmitting and receiving element, are presented and discussed. It is demonstrated that the generated ultrasonic power is sufficient to be revealed by an interferometric acousto-optic fiber receiver.

It is also demonstrated how graphite-like amorphous carbon thin layers, suitable for opto-acoustic generation, are obtainable with thickness around $1\ \mu\text{m}$ and average tolerance of about 5% on a 4 inch wafer while $10\ \mu\text{m}$ thick SU-8 interferometers on silicon substrates have been successfully realized providing a reflectance sensitivity around $13\ \mu\text{m}^{-1}$ with respect to the spacer thickness.



In figure: MOMS opto-acoustic transmitter (left) and receiver (right) mounted on an optical fiber.



In figure a 50 eurocents coin is reconstructed, by elaborating the flight time the ultrasonic pulse. This image was obtained by using two prototypes of MOMS transmitting and receiving elements.

REFERENCES

1. E. Biagi, S. Fontani, F. Francini, L. Masotti, M. Pieraccini, Ultrasonic Symp. 1996 Proc. (1996), 2
2. D. Menichelli, E. Biagi, J. Opt. A: Pure Appl. Opt. (2001), 3
3. E. Biagi, F. Margheri, D. Menichelli, IEEE Trans. Ultrason. Ferroelect. Freq. Contr., 6 (2001), 48.
4. L. Masotti, E. Biagi, F. Margheri, D. Menichelli, U.S. Patent 6 519 376, (Feb. 11, 2003)
5. A. Acquafresca, E. Biagi, L. Masotti, D. Menichelli, IEEE Trans. Ultrason. Ferroelect. Freq. Contr., 10 (2003), 50
6. E. Biagi, A. Acquafresca, S. Cerbai, P. Gambacciani, L. Masotti, Ultrasonic Symp. 2006 Proc. (2006)

DESIGN, FABRICATION AND CHARACTERISATION OF AN ANGULAR VELOCITY SENSOR FOR SPACE APPLICATIONS

C. Ciminelli, F. Dell'Olio, C.E Campanella, M.N. Armenise

Laboratorio di Optoelettronica, Politecnico di Bari, Via E. Orabona n.4, 70125, Bari, Italy.

Abstract

During the last decades photonic technologies for angular rate sensing have enabled the development of very sensitive gyros based on Sagnac effect [1-2].

Integrated optoelectronics for angular rate sensing may solve some open issues in gyro technology such as the need of both weight and size reduction, cost lowering, power consumption decrease, thermal effects limitation, and reliability increase. Photonic technologies could allow the integration of a gyroscope on a single chip and this can be surely pointed out as a very interesting research target especially in the framework of micro- and nano-satellites development.

In passive integrated optical angular rate sensors, an optical cavity is excited by two signals propagating in clockwise (CW) and counter-clockwise (CCW) direction. When the gyro rotates, the resonance frequencies of the cavity relevant to the two propagation directions are not equal. The difference between them is proportional to the angular rate. Passive integrated optical gyros typically employ a large-radius ring resonator having a high quality factor as sensing element. Silica-on-silicon technology allows to fabricate very low-loss (< 0.1 dB/cm) optical waveguides operating at $1.55 \mu\text{m}$. Propagation loss of these waveguides depends also on index contrast Δ between the guiding and the cladding layer and values around $0.01 - 0.03$ dB/cm has been achieved for $\Delta < 1\%$. Bending loss exponentially decreases with curvature radius, so a curvature radius larger than a few millimetres is required to achieve negligible bending loss.

To enhance the quality factor of resonators in silica-on-silicon technology a spiral configuration has been proposed [3-4]. The resonator is coupled to two straight bus waveguides as shown in Fig. 1.

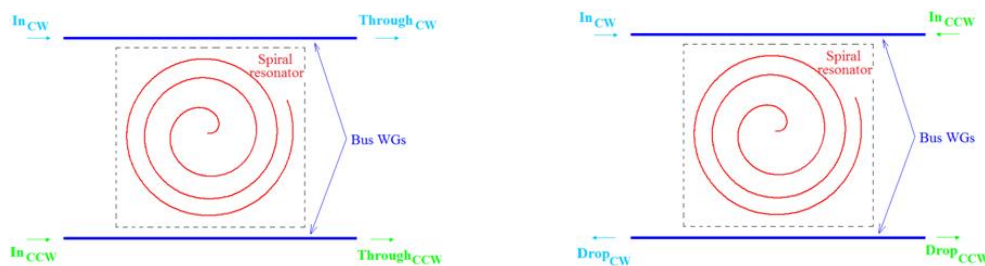


Fig. 1 Through (left) and drop (right) port configuration of the spiral resonator

The spectral response of the cavity has been derived by using the transfer matrix method, neglecting the coupling effect due to the interaction of the two counter-propagating modes because they are supposed to be not simultaneously launched in.

The minimum detectable angular velocity ($\delta\Omega$) of a passive ring resonator gyro is limited by the shot noise at the photodetector included in the read-out system and is expressed as

$$\delta\Omega = \frac{2\pi}{L} \frac{1}{\sqrt{\eta P}} \frac{\sqrt{hc^3 B}}{\sqrt{2\lambda}} \frac{1}{Q\sqrt{\rho}}$$

where λ is the operating wavelength, c is the light velocity in the vacuum, h is Planck's constant, P : optical power coming in the photodetector, B is the sensor bandwidth, η is the photodetector quantum efficiency, L is the spiral length, Q is the resonator quality factor and ρ is the resonance deep. To reduce $\delta\Omega$, Q needs to be increased as well as the resonance deep.

Both resonance deep and quality factor as a function of the spiral resonator length (ranging from 1 to 40 cm) and the power coupling coefficient K between the resonator and the bus waveguides (in the range 0.1-30 %) have been investigated. Propagation loss of the silica-on-silicon waveguide ($= 0.1$ dB/cm) and guiding structure effective index ($= 1.457$) have been kept constant.

To reduce the detection limit, a good agreement between quality factor and resonance deep have to be assured for each possible configuration (drop port and through port). Fig. 2 shows the results of the parametric analysis on Q by changing the resonator length and the coupling coefficient. Calculations have been carried out also for ρ , for both through and drop port configurations.

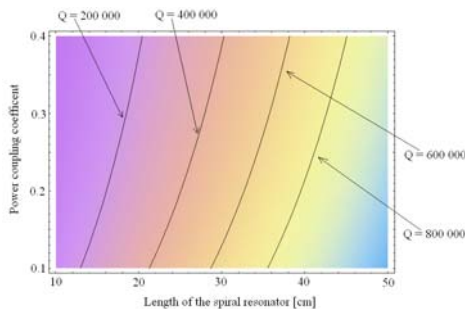


Fig. 2 Quality factor as a function of power coupling coefficient and spiral length

By assuming a spiral length longer than 30 cm, quality factors higher than 10^6 are achievable although the resonance deep cannot be optimized at the same time. However, since Q factor influences the sensitivity much more than ρ , the spiral has been designed to optimized it. A resolution in the range 10 - 100 $^{\circ}/h$ can be obtained by using a waveguide with propagation loss equal to 0.1 dB/cm.

By reducing propagation loss until 0.01 dB/cm, the resolution can be lowered to the range 1 – 10 $^{\circ}/h$. As an example, for a resonator length of 38.4 cm the sensitivity is 28.5 $^{\circ}/h$ when propagation loss is 0.1 dB/cm and the coupling strength is 20 %. By assuming the same length, sensitivity becomes 14.8 $^{\circ}/h$ when propagation loss is 0.05 dB/cm and the coupling strength is 10 % and 3.0 $^{\circ}/h$ for propagation loss of 0.01 dB/cm and coupling strength of 2 %.

The spiral resonator has been fabricated by using silica buried waveguides with a core size of $6 \times 6 \mu\text{m}^2$ and an index contrast of 0.75% at $\lambda = 1.55 \mu\text{m}$. Fig. 3 shows the experimental results obtained for a 42 cm long spiral having through configuration, with a coupling coefficient of 40 %.



Fig. 3. Experimental spectrum of a 42 cm long spiral resonator.

From the measured spectrum a quality factor Q equal to $1.55 \cdot 10^6$ has been calculated. This result, better than the simulated Q value ($= 1.4 \cdot 10^6$), is due to the lower propagation losses of the fabricated waveguides estimated to be about 0.08 dB/cm. Thus, a sensitivity value of about 10 $^{\circ}/h$ has been demonstrated.

REFERENCES

1. M.N. Armenise, V.M.N. Passaro, F. De Leonardis, M. Armenise, "Modeling and Design of a Novel Miniaturized Integrated Optical Sensor for Gyroscope Applications", *J. Lightwave Technology*, 19, pp. 1476-1494, 2001.
2. C. Ciminelli, C.E. Campanella, M.N. Armenise, "Optimized Design of Integrated Optical Angular Velocity Sensors Based on a Passive Ring Resonator", *J. Lightwave Technology*, 27, pp. 2658-2666, 2009.
3. "Integrated-Optics Laser Gyro Technology (IOLG)" ESA/ESTEC - MI CONTRACT n. 16782/02/NL/PA.
4. C. Ciminelli, C.E. Campanella, F. Dell'Olivo, V.M.N. Passaro, M.N. Armenise, "A novel passive ring resonator gyroscope", Joint Meeting, Brescia, 2 - 5 June 2009.

SUPERCONDUCTIVE MAGNETOMETER AND GRADIOMETER FOR LARGE MULTICHANNEL BIOMAGNETIC SYSTEMS

A. Vettoliere, C. Granata, M. Russo

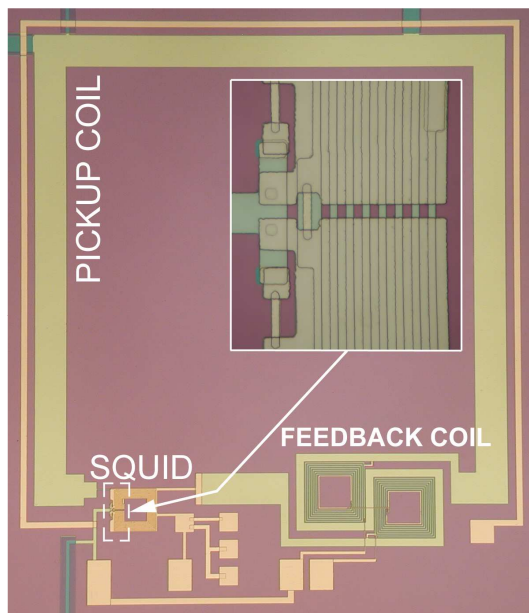
Istituto di Cibernetica "E. Caianiello" del CNR, via Campi Flegrei, 34, 80078 Pozzuoli (NA), Italy

Abstract

A niobium based dc-superconducting quantum interference devices (SQUIDs) for high magnetic field sensitivity applications have been developed.

In particular, we present a miniaturized dc-SQUID magnetometer having an integrated superconductive sensing coil in a square shape with a side length of 3 mm, involving a device area much smaller than a standard SQUID magnetometers with a comparable magnetic field sensitivity; In such a way the spatial resolution is increased maintaining the required magnetic field sensitivity. Moreover, a small pickup coil minimizes its antenna gain, reducing the radio frequency interference. The measurements performed in Flux Locked Loop (FLL) configuration and at T=4.2 K, have shown smooth and resonance free Voltage-Flux (V- Φ) characteristics and an intrinsic magnetic field noise spectral density of 5.8 fT/Hz^{1/2} in the white region. The good agreement with the theoretical predictions guarantees the reliability and the controllability of these sensors.

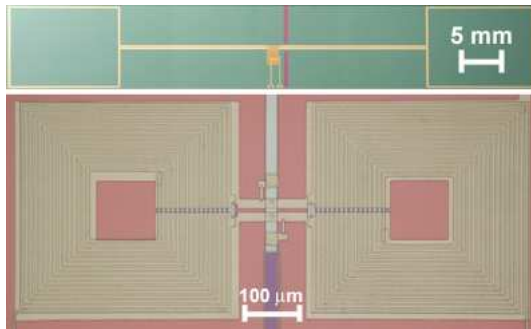
Due to their compactness and good characteristic parameters, such sensors are suitable for large multichannel systems used in biomagnetic imaging.



Picture of a fully integrated SQUID magnetometer. In the inset, the magnification of the Josephson junctions, shunt and damping resistors is shown.

A planar SQUID gradiometer is also presented. Its pickup antenna consists of two integrated rectangular coils connected in series, having a long distance between their center (baseline) equal to 50 mm; it is magnetically coupled to a dc-SQUID, in a double parallel washer configuration, by two series of multiturn input coils.

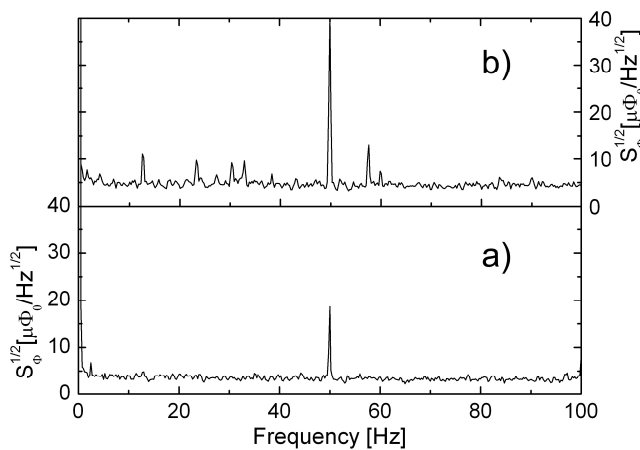
The sensors have been designed and fabricated to achieve a high intrinsic responsivity, they have shown, at $T=4.2$ K and in the Flux Locked Loop operation mode, a white spectral density of magnetic flux and field noise equal to $3 \mu\Phi_0/\text{Hz}^{1/2}$ and $3 \text{ fT}/\text{Hz}^{1/2}$ respectively, resulting in a gradient spectral noise of $0.6 \text{ fT}/(\text{cm}\cdot\text{Hz}^{1/2})$.



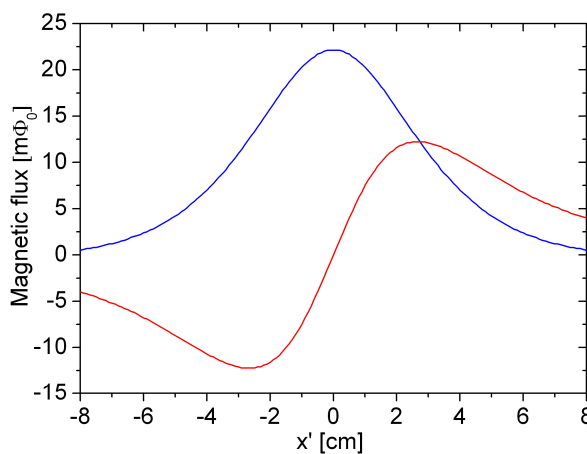
Picture of a fully integrated SQUID gradiometer (upper figure) and the SQUID in the parallel double washer configuration (lower figure).

In order to verify the effectiveness of such sensors for biomagnetic applications, the magnetic response to a current dipole has been calculated and the results have been compared with those of an analogous axial gradiometer.

The results show that there is no significant difference. Due to their high intrinsic balance and good performances, planar gradiometers may be the elective sensors for biomagnetic application in a soft shielded environment.



Spectral densities of the magnetic flux noise of a planar SQUID gradiometer (a) and a SQUID magnetometer (b) measured at $T=4.2$ K in FLL configuration.



Output magnetic fluxes of a planar (blue line) and an axial (red line) SQUID gradiometer as function of the off-axis position x' . The current dipole strength is $p_y=10 \text{ nA}\cdot\text{m}$ and its distance from the sensor is $D=4 \text{ cm}$.

REFERENCES

1. C. Granata, A. Vettoliere, M. Russo, Appl. Phys. Lett., 91, 122509 (2007)
2. C. Granata, A. Vettoliere, C. Nappi, M. Lissitskiy, M. Russo, Appl. Phys. Lett., 95, 042502 (2009)
3. R. Cantor, J. Ad Hall, A. N. Matlachov, and P. L. Volegov, IEEE Trans. Appl. Supercond. 17, 672 (2007).

POWER MANAGEMENT SYSTEMS FOR PHOTOVOLTAIC ENERGY HARVESTERS

M. Ferri, D. Pinna, M. Grassi, E. Dallago, P. Malcovati

Department of Electrical Engineering, University of Pavia, Via Ferrata, 1 27100 Pavia

Abstract

Integrated systems are constantly improving in terms of functionalities and computational capabilities [1], [2]. On the other hand, the battery energy density is not improving with the same speed and battery life is becoming in many cases a real bottleneck, especially for portable applications [3], [4]. Energy harvesting systems are becoming the new challenge in both commercial and research communities as alternative, or additional, power source. In many cases, in fact, the final application operates in environment with many energy sources, such as light, vibrations or thermal gradients. In this case energy harvesting represents an optimum option to increase the performance of the device, reducing its volume and weight. Light can be considered the most copious energy source in most environments, thus making the photovoltaic energy harvesting the largest contribute to the power supplying process. When the electronic circuits required for the power management system has to be implemented on the same chip of the photovoltaic energy harvesting elements, the choice of the fabrication technology of the microsystem is subordinated to the final application, leading to a trade-off between costs and feasibility. In this paper we present two different solutions of integrated photovoltaic energy harvesting, realized for discrete and continuous time working systems. The first solution is realized in a cheap standard $0.35\mu\text{m}$ CMOS technology, while the second in $0.35\mu\text{m}$ SOI CMOS technology.

Figure 1 shows the microphotograph and the block diagram of the chip implementing the first solution, where a generic resistive load has been considered.

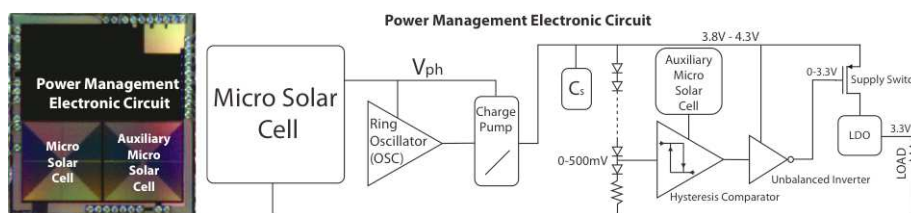


Figure 1. Micro-photograph and block diagram of the energy harvester in $0.35\mu\text{m}$ CMOS technology for discrete-time working microsystems.

The main problem of this solution, and of all those where insulation is guaranteed by the reverse biasing of the substrate connected junctions, is the impossibility to create series of solar cells on the same silicon wafer. The common presence of the substrate, in fact, introduces photoelectric phenomena also for the parasitic junctions [5]. For this reason the circuit presented in Figure 1 elevates with a charge pump the photogenerated voltage of a single solar cell and charges an external capacitor, in order to supply with 3.3V, through a linear voltage regulator (LDO), the load for a given time-slot, in asynchronous discrete-time regime. The time-slots dedicated to energy accumulation and system operation are established automatically by the system.

With this solution it is possible, by choosing the value of the external capacitor, to trade the amount of power available for the load with the time required to accumulate it, thus allowing to supply the

load for the required time-slot with the required current with a given duty-cycle. The proposed power management circuit consists of an hysteresis comparator and an unbalanced inverter, that controls a switch to connect the load to the storage capacitance. The comparator monitors the charge voltage on the storage capacitor. When the stored charge is sufficient to reach a voltage equal to 4.3 V the comparator provides a signal that, by means of the unbalanced inverter, connects the LDO to the supply voltage (i. e. the storage capacitor), thus supplying the load. When the external capacitor discharges, and the voltage decreases below 3.8V, the load is disconnected, and, so, switched off.

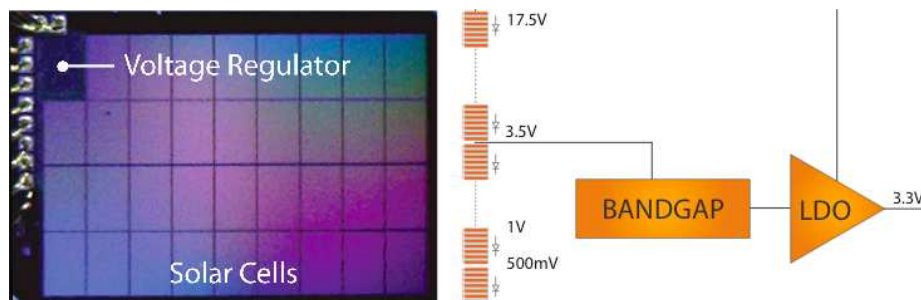


Figure 2. Microphotograph and block diagram of the energy harvester in 0.35 μ m CMOS SOI technology for continuous-time working microsystems.

Figure 2 shows the microphotograph and the block diagram of the photovoltaic energy harvester realized in 0.35 μ m CMOS SOI technology for continuous-time working microsystems. This solution consists in a series of 35 trenched p-n junction, a bandgap device and an high voltage LDO. This regulator allows to provide a fixed 3.3V, also in low environment illumination conditions, as the large number of micro photo-structure chain allows each cell to decrease its voltage of almost 20%, when the power curve changes for illumination variations, or larger load power request than typical. In this solution the series connection of the micro solar cells has been available because of the oxide trenches around the well that physically insulates them from the common substrate. On the other hand, this fabrication technology is more expensive than the standard CMOS.

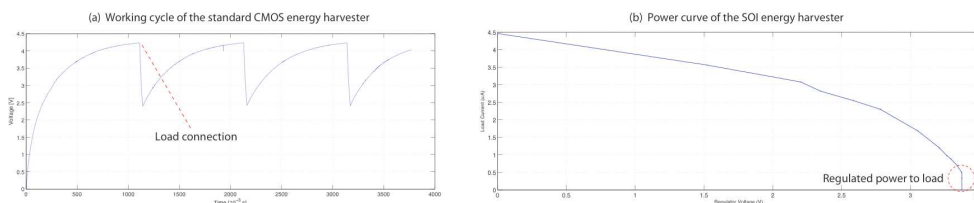


Figure 3. (a) Standard CMOS harvester working cycle and (b) SOI harvester power curve.

Figure 3.a shows an measured working cycle of the standard CMOS solution, while Figure 3.b shows the power curve referred to the SOI photovoltaic energy harvester. Both solution have been realized on chip and completely characterized experimentally.

REFERENCES

1. W. Andre and S. Martel, "Preliminary design of an autonomous microrobot propelled by magnetotactic bacteria," in Proceedings of IEEE/ASME International Conference on Advanced Intelligent Mechatronics, Sep. 2007, pp. 1–6.
2. H. L. Ho, M. D. Steigerwalt, B. L. Walsh, T. L. Doney, D. Wildrick, P. A. McFarland, J. Benedict, K. A. Bard, D. Pendleton, J. D. Lee, S. L. Maurer, B. Corrow, and D. K. Sadana, "A 0.13 μ m high-performance SOI logic technology with embedded DRAM for system-on-a-chip application," in IEEE International Electron Devices Meeting (IEDM) Technical Digest, Dec. 2001, pp. 22.3.1–22.3.4.
3. J. Gao and L. Yu, "Use of battery ohmic testing to improve network reliability and decrease battery maintenance cost," in Proceedings of International Telecommunications Energy Conference (INTELEC), Oct. 2007, pp. 194–202.
4. D. Dondi, D. Brunelli, L. Benini, P. Pavan, A. Bertacchini, and L. Larcher, "Photovoltaic cell modeling for solar energy powered sensor networks," in International Workshop on Advances in Sensors and Interface (IWAS), Jun. 2007, pp. 1–6.